Scientific Research Publishing

Journal of Modern Physics, 2025, 16(6), 911-932
https://www.scirp.org/journal/jmp
ISSN Online: 2153-120X
ISSN Print: 2153-1196

Physical Quanta in Quasicrystal Convergent Beam Electron Diffraction

Antony J. Bourdillon

UHRL, San Jose, CA, USA
Email: bourdillona@sbcglobal.net

How to cite this paper: Bourdillon, A.J. (2025) Physical Quanta in Quasicrystal Convergent Beam Electron Diffraction. *Journal of Modern Physics*, **16**, 911-932.
https://doi.org/10.4236/jmp.2025.166047

Received: March 18, 2025
Accepted: June 27, 2025
Published: June 30, 2025

Abstract

This paper serves two purposes. *Firstly*, we show how the classical mechanics of Newton—where momentum energy is less than rest mass energy, $pc \ll m_o c^2 = E_o$—transitions with increasing momentum, to the relativistic mechanics of Einstein and Klein-Gordon, where $pc \gg m_o c^2$. To describe the transition, we replace the classical rest mass energy constant E_o by Einstein's varying relativistic energy $E = m'c^2 = \sqrt{p^2c^2 + m_o^2c^4}$, and apply it to dispersion dynamics in the electron microscope. *Secondly*, we show how diffractive wave mechanics enables unconventional *logarithmic* order in hierarchic quasicrystals. This order acts simultaneously to produce conventional dynamical interference in *linear* order. Each of these remarkable physical effects is explained with neither abstruse mathematics nor arbitrary inventions of dimensionality; but in a realistic framework of conventional and verified hypotheses. The results describe momentum quanta in scattering by free electrons that resonate with dual diffraction in quasicrystalline *convergent beam electron diffraction*. Here, irrational indices in the quasicrystals separate into real and imaginary parts, where the latter part shifts the phase of the free-particle wave-function. The shift provides a new constant, a log-lin metric function, in the physics of condensed matter. The phase shift also demonstrates superposition of scattered rays simultaneously into both *logarithmic space and linear space*. The dual diffraction occurs, in dynamical diffraction by virtue of a "quasi-Bloch-wave" that is deduced from parallel beam diffraction and confirmed by its results in Convergent Beam Electron Diffraction. The momentum quantum resonates with multiple effects that are not simply reducible to chance.

Keywords

Wave Packet, Phase Velocity, Group Velocity, Dispersion Dynamics, Quantum, Dual Resonance, Quasicrystal, Log-lin Metric, CBED

1. Introduction

We re-interpret earlier experimental results to confirm the dual logarithmic and linear harmonies that are evident in quasi-Bragg diffraction from icosahedral quasicrystals. These solids constitute a comparatively new structure in matter that is weakly periodic in geometric series. Their sharp diffraction patterns are observed after scattering by a periodic probe, either x-ray or electronic, into diffraction patterns in geometric series. The series are 3-dimensional, ordered by τ^m, $m = -1, 0, 1, 2, 3\ldots$ The series is also Fibonacci, seeded $F(1, \tau)$, where the golden section $\tau = \left(1+\sqrt{5}\right)/2$, *i.e.* irrational [1] [2] (**Appendix 1**). The series are not consequences of Bragg diffraction in crystals[1], where all of the probe, the crystal, and the diffraction pattern, are linearly periodic with integral orders, $n \geq 0$. Analysis by modified structure-factors, and measurements of the quasi-lattice-parameter demonstrate diffracted beams displaced from corresponding Bragg spectra by a coherence factor, $c_s = \left(\tau - 1/2\right)^{-1}$, that has the extraordinary property of being identical in all diffracted beams from a quasicrystal (QC). The factor is the same constant whether analytical, numerical or experimental. The factor expresses a separable irrational part of the particular index of a diffracted beam. It represents a new constant in condensed matter physics, and is unique to icosahedral structures. Moreover, the diffracted beam is found, by conventional interpretation, to be composed of dual harmonies in quasi-Bloch-waves. The harmonies are both logarithmic and linear (log-lin); both long range and short range; part rational and part irrational. The extraordinary dual harmonies explain—after separation of the irrational parts from integral parts—scattering of the *periodic* incident probe, off the *hierarchic* structure, onto the *geometric* diffraction pattern. We analyze a convergent beam electron diffraction pattern (CBED) [3] for the first time, following the complete structural study of parallel beam logarithmic quasicrystal diffraction. The solution demonstrates several types of wave superposition.

Moreover, this geometric pattern is a quantum effect in *momentum space*. Its dual harmony demonstrates fundamental features of quantization, *i.e.* the well-known phenomena reported by Planck in black-body spectra, and by Einstein in the photo-electric effect, both in *energy space*. A single harmony, as in X-ray and electron diffraction from *crystals*, leaves the nature of the momentum quantum open to interpretation; *but in QC diffraction, the dual harmony and dual log-lin interaction demonstrate that dual resonance is the physical origin of the quantum*. Resonance is an old physical characteristic that makes the recognition of the photonic quantum not as a leap, but as more of the same: for example in Schrödinger's hydrogen atom, a decay between a harmonic excited $2P_{3/2}$ state to the $1S_{1/2}$ harmonic ground state. The transition is, and always was, as physical as falling apples: particularly as dispersed in time; and not instantaneous as in mathematical quantum mechanics.

Likewise, periodic Bragg diffraction can be interpreted in more than one way

[1] $n\lambda = 2d\sin(\theta)$, where n is the integral order; λ the probe wavelength; d the crystal's inter-atomic spacing; and θ the Bragg angle.

to include quantization; but our dual diffraction, that is partly (linear) Bragg diffraction and partly (logarithmic) quasi-Bragg diffraction, is by contrast definite: the fact of dual diffraction in convergent beam electron diffraction (CBED) in QCs, will prove to be further evidence for, and formal explanation of, the fact that *all quanta in atomic physics are caused by physical resonances*—whether they are also arithmetic axioms or not.

There is a misunderstanding where clarity is needed [4]: is the quantum math or physics? Von Neumann's book is entitled *Mathematical foundations of quantum mechanics* [5]; Popper's is *Quantum theory and the schism in physics* [6]. The specific logics are opposites. How falsify axioms [7]? This paper is not about 2-dimensional tiling of an infinite aperiodic surface; there is no evidence for that. The paper is about the 3-dimensional atomic structure of quasicrystals, typically observed on arbitrary electropolished slices when they are, in principle, defective. The atoms themselves are typically extremely restricted, being of only two species, in our case: *Al* and *Mn*, in stoichiometric ratio 6:1. Before allowing for chemical bonding in outer electrons in the metallic alloy, each species has its own unique diameter.

We have first to understand the unique diffraction. An extended purpose is to engineer electronic, chemical and mechanical properties. Popper's method of falsification is necessary in physics, fundamentally because Immanuel Kant's *Ding an sich*[2] can never be completely known. The best we can do in physics is to empirically falsify hypotheses, so as to narrow possibilities *i.e.* by falsifying predictions. We employ the physical wave-group description for the free particle quantum. It is not a point particle[3] and so cannot interact instantaneously. Besides references to all necessary information, three appendices are provided for general background in quasicrystals and electron microscopy.

2. CBED

2.1. Quasicrystal Convergent Beam Electron Diffraction

Figure 1 shows a clear, schematic representation of a remarkable experiment that was executed some years ago [3] and that is *now* reinterpreted. The improvement is made possible by the complete description that we have meantime developed for both the structure of quasicrystals (QCs) and of their diffraction mechanism [1]. Though the structure of Al_6Mn displays sharp diffraction in parallel beam incidence, with icosahedral symmetry; it is not crystalline; does not obey Bragg's law; is 3-dimensional [8]; is hierarchic; has translational symmetry (cf. [9]) in geometric series; and contains new physics in its irrational, (log-lin) metric function. The function is unique to the hierarchic, icosahedral structure. The experiment provided a convergent-beam electron diffraction pattern (CBED) of an electropolished thin film of quasicrystalline Al_6Mn. Here, its five-fold axis (forbidden

[2]Translated, *Thing in itself*, *i.e.* beyond sensory phenomena (and experiment).

[3]Because electron optics are the same as light optics after minor adjustments for mass, charge, spin and polarity.

in crystals) is parallel to the axis of the incident beam. The normal diffraction spots that are evident in (parallel beam) Bragg diffraction, are expanded by beam convergence at the specimen with divergence away from it, into illuminated circles in the back focal plane of an electron microscope. These circles contain noteworthy sub-structures that further confirm the log-lin behavior that had been evident in the former description of the QC structure and parallel beam diffraction (**Appendix 1**) [1].

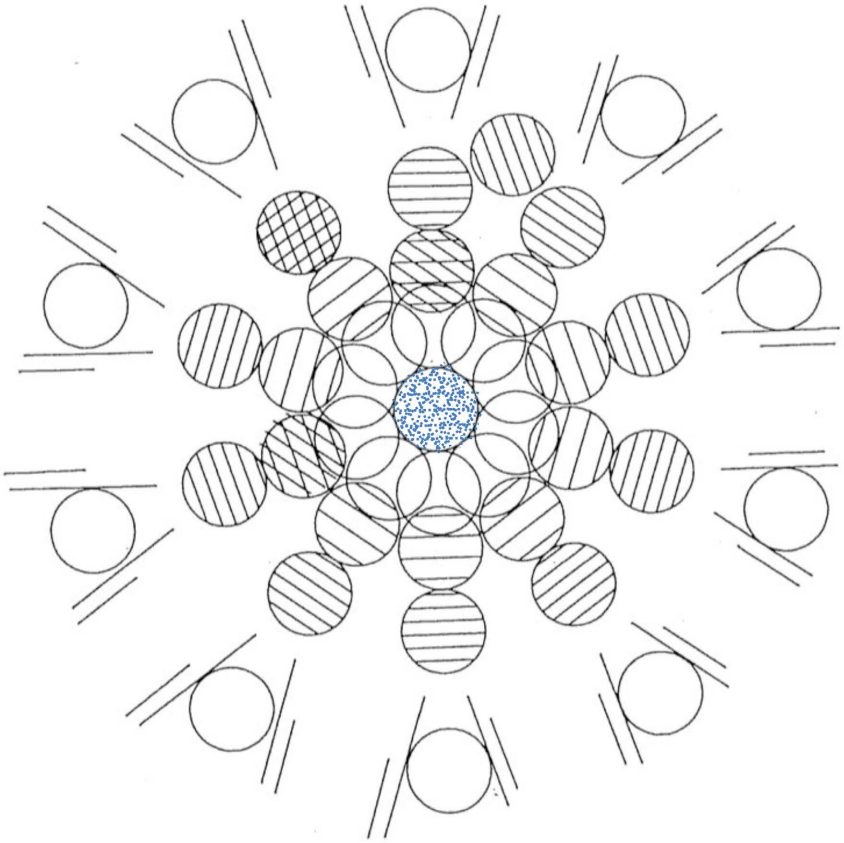

Figure 1. Schematic diagram of axial pattern structure recorded [3] in Convergent Beam Electron Diffraction from icosahedral Al_6Mn oriented with a five-fold [τ01] axis parallel to probe [8]. Indices of the diffracted beams, upwards on the vertical axis, from the center, are (000), (0τ^{-1}0), (010), (0τ0), and (0$\tau^2$0) *i.e.* in *geometric series*. A dense fringe structure is present in the zero order beam that pair with individual structures in the second and third 10-fold *ring* of *circular* diffracted beams. Inside many of the individual beam intensities in the geometrically spaced beams, there are *linearly* spaced fringes with spatial frequencies that are proportional to the dominant scattering angles. Seemingly random cross fringes also appear about pairs of beams. The most remarkable fact is the occurrence of *combined scattering of the logarithmically indexed beams* with *regularly spaced fringe structure within individual beams*. Most often, the fringes pair with the schematic criss-crossed hairlines in the central (000) beam, that roughly replicate the original micrograph.

CBED is a mature branch of electron microscopy [10] [11]. The point of convergence at the specimen, expands into divergent circular patterns on the back focal plane. The electron beam is treated as monochromatic, but the diffraction

pattern is spread like an X-ray Laue pattern partly because the wavelength is typically much shorter than atomic separations in the scattering specimen, and partly because of the comparatively strong scattering power of electrons. This is a well-known difference between X-ray and electron spectrometry. In CBED, the incidence is set parallel to a Laue zone axis and information is recorded over zeroth order, first order and Higher Order Laue Zones (HOLTZ). Generally, within the individual circles, complicated fringes and lines occur that are related to atomic potentials and to atomic planes. The patterns are used to identify phases in alloy specimens [10].

CBED structure varies with specimen thickness. This is typically measured, in dark field or bright field in the usual way, by thickness fringes in wedge foils. These fringes result from scattering in the two beam condition by dynamical diffraction between the zero-order beam and diffracted beam. The fringes discussed in this study appear to be due to the same mechanism but are peculiar to quasicrystals: in both cases the fringes are paired in matching beams (typically the zero-order and diffracted beam).

2.2. The Dominant Diffraction Is in Geometric Series

The convergent beam diffraction in the quasicrystal, that was observed and is illustrated schematically in **Figure 1**, displays fringes that obey *two separate laws of physics*, *neither of them Bragg diffraction*. The dominant structure satisfies the quasi-Bragg law (**Appendix 1**) [1] in geometric series for the *axis* of the diverging beam, within the envelope $|\zeta| \le |Z|$, where Z is the angle subtending the convergent probe. Then:

$$\tau^m \lambda = 2d' \sin\left(\theta'\right) \tag{1}$$

where λ is the wavelength of the monochromatic probe; $d' = c_s \cdot d$ the effective crystallographic quasi-d-spacing that is modified by the coherence factor c_s; and θ' the quasi-Bragg angle. Simultaneous secondary structures in linear order are also observed, $n\lambda = 2d\sin(\theta)$. This fact is analyzed to confirm the *dual harmonies* previously described as quasi-Bloch waves. Further details are illustrated in **Appendix 1**.

Following those observations, **Figure 2** illustrates a blue *crystalline* Bloch wave due to the superposition of the zero order beam and a diffracted beam in the two beam condition [12]. The Bloch waves are generated by conventional dynamical diffraction in crystalline specimens. The waves are commensurate with the unit cell and with periodically repeating cells, and such waves are regularly used to form lattice images. In QC diffraction, the Bloch wave is stretched by the metric function $c_m = c_s^{-1}$ to provide the red quasi-Bloch-wave. As the figure shows, the wave is logarithmically periodic and commensurate with the hierarchic quasi-lattice in long-range; and linearly periodic about each logarithmic intercept in short range.

The coherence factor c_s (**Appendix 1**, **Figure A3**) is the principal feature of this study for many reasons: it applies universally across all diffraction beams from the

icosahedral structure; it is extensively calculated by numerical methods; it is systematically and analytically derived; and moreover it explains the coherent diffraction from the aperiodic structure; all while it is necessary for measuring the quasi-lattice parameter that was used to verify the structure and method.

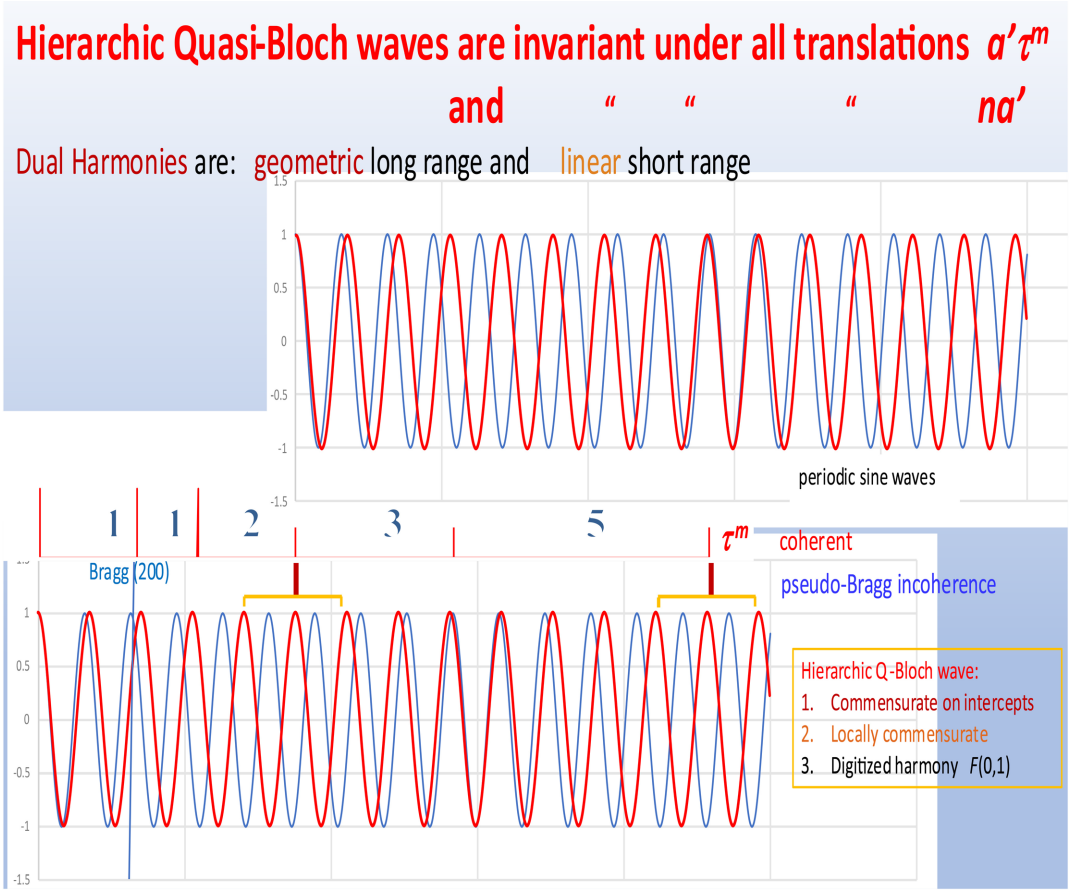

Figure 2. Comparison of a the blue Bloch-wave that is linearly periodic in crystals with the red quasi-Bloch wave that is logarithmically periodic in QCs in long range, while being linearly periodic in short range. The log-lin metric[4] stretch in the latter wave is given by $c_s^{-1} = 1.118034\cdots = \tau - 1/2$. This number is simply the irrational part separated from irrational indices shown, as examples, in appended **Figure A1** and in the indexed planes in **Figure A2**.

Without c_s, no researcher has demonstrated the physical process of 3-dimensional, geometric series diffraction in quasicrystals. The derivation that we give has been computed for ~100 diffraction lines with programs written in double (128 bit) precision; on code that is iterative over ~10^8 atoms in some cases; takes hours to run; and that has been described in 8 monographs and 28 journal articles [13] that include long lists of indexed patterns with corresponding beam intensities (*e.g.* [2]. Moreover, the metric function $1/c_s$ has been mathematically, systematically and clearly derived out of the separable irrational, icosahedral indices, us-

[4]©Smithsonian SAO Astrophysics Data system, Mail: adshelp[at]cfa.harvard.edu, *The Log-lin Metric for Generic Responses in Logarithmic Structures,* Bourdillon A.J., APS March Meeting (2015), abstract id.W15.014B Bibcode 2015APS.MARW15014B.

ing an adaptation of classical Bragg diffraction to the hierarchic structures, as in **Appendix 1**. The results match, coherently, both the diffraction intensities and typical optimum defocus images with which they are compared [2]. The derivation of c_s can hardly be more thorough.

Figure 2 shows that the corresponding abscissae axis of the crystal Bloch wave, when simply stretched by the log-lin metric function $c_m = \tau - 1/_2 = 1/c_s$ (**Appendix I**), to yield the quasi-Bloch wave that has both logarithmic and linear periodicities. This procedure had been previously justified by the geometric series results of parallel-beam quasi-Bragg diffraction; it now applies to the CBED quasi-Bloch waves because it is already known and verified.

In crystals oriented to the two beam condition, the Bloch wave is generated by the removal of a degeneracy in *momentum wave-bands* at crossover between zero order and diffracted beams [12]. Without exchange of energy, the waves acquire different wavelengths from crystal potentials, and thereafter interfere. The fringes occur by a pendulum effect as the Bloch wave advances through a crystal. The interference is observed below the crystal surface, typically after the zero-order beam and diffracted beam separate. *In quasicrystals*, angular divergences between the two beams occur on logarithmic scale instead of linear scale. The difference has been described for bands in energy space and momentum space [2], but is not significant for dynamical diffraction in the fringe substructures of Figure 1: the fringes are linearly spaced as is typical in dynamical diffraction.

2.3. Fringe Patterns in the Second and Third Rings

Outside the central (000) zero order beam, oriented parallel to a 5-fold axis in Figure 1, diffracted beams are arranged in concentric rings (corresponding to **Appendix I** Figure A1, lower row, as measured in parallel beam). The third ring of beams is the brightest because its calculated QSF corresponds to the dominant inter-cellular spacing in the hierarchic structure, *i.e.* to the $(0\,\tau 0)$ diffraction index (**Appendix 1**) and nine other beams on the same radius [2].

The second ring is not as bright but corresponds to the width of the unit cell and quasi-lattice-parameter, *i.e.* to the (010) index [1]. The parameter has the same length as the Al atomic diameter, as in the structural model used in the calculation. The first ring has the shortest radius, from (000) to $(0\,\tau^{-1}0)$, and is comparatively weak.

Spectacular fine structures occur within the second and third rings. The parallel line structures cross at right angles to the dominant geometrically diffracted beam axis. They lie in linear order with spatial frequency proportional to the dominant scattering angle $\Theta' \approx 2\theta'$ since $\theta' \ll \tau^m \lambda / 2d'$. The combined law of diffraction may therefore be written approximately:

$$\Theta \approx \frac{\tau^m \lambda}{d'} \cdot \frac{n}{d} \tag{2}$$

conditional on the convergence $|\zeta| < |\mathcal{Z}|$. In the present case it appears that, very roughly, $d \approx d'/3$ and the spatial frequency of the fringe is 6x greater than the

dominant axial diffraction angle of the second or third rings respectively. Fringes of this type are common in CBED [10] [11]; but only in this work is there confluence with the dominant logarithmic diffraction.

2.4. Fringe Patterns in the Zero Order Beam

The central, zero order (000) beam is, in the original data [1], actually the most intense of all the recorded beams, as is typical in CBED from films that are sufficiently thin. In crystals, the intensity of diffracted beams generally falls as the scattering angle increases, chiefly owing to increasing deviation parameter (the distance between a point on the Ewald sphere and the back focal plane) until the first order Laue zone is reached.

However, the zero order beam is not uniformly illuminated: the original data [3] show ordered, cris-crossed, hairline striations that complement hairlines in the second and third ring of circles in **Figure 1**. These striations are evidence for pendelösung (pendulum) scattering due to dynamical diffraction [13] in the zero-order beam, oscillating with the diffracted rays in the second and third rings. In these two rings, the spatial frequencies of the fringes are proportional to their quasi-Bragg angles: they are τ times larger in the third ring compared to the second.

Dynamical diffraction is used to understand many contrast features in crystals, and is obviously the mechanism that causes the complementary hairlines in the zero order and other beams. It causes a beam to interact with a crystal (and as we find in the QC) by Bloch waves that are superpositions of the zero order beam with corresponding diffracted beams.

This description is consistent with the symmetries that appear in the zero order and with the 10-fold symmetries in the second and third order rings. However, some structures, beyond 10-fold, are also observed, as in Section 2.6.

2.5. Dynamical Diffraction of Quasi-Bloch Wave Components by Virtue of the Metric Function in Hierarchic Quasicrystals

In the electron microscopy of thin crystals [12], three diffraction theories are principally used to identify contrast mechanisms that are evident in imaging. They are Bragg-diffraction, kinematic theory and dynamical theory. In addition, the broad field of specimens applies many specialized techniques including Lorentz microscopy for magnetic specimens.

Bragg-spectrometry started in X-ray laboratories, and the groundwork is adapted, *mutatis mutandis*, to electron imaging and diffraction, especially for perfect crystals. This diffraction theory extended to minor phases: kinematic theory applies when amplitudes of diffracted beams are much smaller than the amplitude of the incident beam; Typically, this occurs where scattering atoms are far apart or when atomic form factors are reduced by large scattering angles. In dynamical diffraction, diffracted amplitudes are of the same order as the amplitude of the original incident beam. The diffracted beams then further defract. The simplest case is the two beam condition illustrated in **Figure 3**. The two beams mutually

annihilate and create the other. They do so repeatedly: in wedge foils: up to 10 cycles are often seen as repeating fringes in either bright field or dark field. When the extinction distance for the fringes is known [12], the foil thickness is measured and this is often a critical parameter in image interpretation. The fringes that appear in **Figure 1** and **Figure 3** are of this type but adapted to convergent beam incidence. In this case the atomic scattering amplitude [12] varies across the diverging disc in the back focal plane, *i.e.* consistently with the divergent angle about the central ray and with Equation (2). The fringes in the bright field (000) are complementary to the corresponding dark field (τ00) beam.

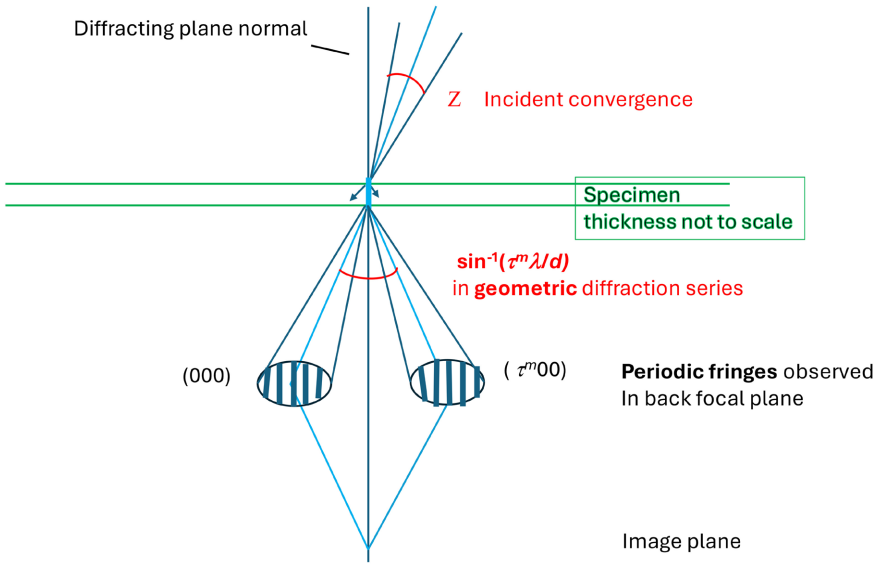

Figure 3. Schematic diagram showing dynamical diffraction in the two beam condition due to a convergent incident beam. Inside the specimen, arrows indicate different wavelengths of the diffracted beam relative to the central ray of the incident beam. The dual, logarithmic and linear diffraction, and dual quantization is enabled by the dual quasi-Bloch wave in **Figure 2**. The figure illustrates Equation (2).

The fact of dynamical diffraction reinforces the quasi-Bloch wave application in QC diffraction:

Firstly, superposition of the pair of beams in the hierarchic structure, follows their earlier explanation in crystals: between the two beams, their *momentum band structures* split at their crossover where degeneracy is removed ([2], pp. 15-17), so that the probe wavelengths differ in the two beams. These interfere [11] in the solid structure before exiting the lower quasicrystal surface. Complementary fringes are observed in bright field (000) and in dark field (diffracted beam). The splitting is consistent with the metric function c_m and with dual log-lin quasi-Bloch-waves, since the quasi-Bloch wave (**Figure 2**) has *both linear and logarithmic periodicity*. The function had first been demonstrated in structural studies by parallel beam microscopy, and verified by quasi-lattice measurements. *There*, *quasi-Bloch waves were deduced; now*, *CBED provides visual evidence*.

Secondly, the pendulum complementarity in fringes between the *zero order* and

logarithmically diffracted beams is the consequence of quasi-Bloch-wave interference as wave pairs advance through the QC specimen and emerge at the lower surface of the specimen foil where the zero-order beam and diffracted beams superpose and interfere.

In summary

The fringes are due to interference between pairs of beams (typically one transmitted (000); the other Bragg-scattered (τ^m00)) advancing through a specimen. The beams have equal energy but different momenta on non-degenerate momentum bands. The beams swap momenta like a swinging pendulum as they advance; and eventually exit the specimen with complementary, alternating amplitudes, having hills snd valleys across their divergent cross-sections. Before the pair separates from the specimen, it forms a Bloch wave. Figure 1 contains a spectacular, ten-fold, zone-axis display. The dual logarithmic and linear harmonies in the quasi-Bloch waves (Figure 2), enable the periodic fringes within the geometric quasicrystal diffraction.

2.6. Fringe Patterns in Other Beams

Further fringes in the second ring beam at 8 o'clock in Figure 1, complement fringes in the third ring at 12 o'clock. Also, fringes in the third ring beam at 11 o'clock complement the forbidden beam outside the third ring. We suppose these are consequences of slight misalignment of the incident beam with the QC axis. Whatever the detail, the patterns confirm, as before, pendulum scattering between two beams by double diffraction.

2.7. Dual Harmonics in Quasi-Bloch Waves

The diffraction beam, that interferes to form both the logarithmic pattern and the linear fringes, interacts with the hierarchic quasicrystal via a metric that is unique to quasicrystals. Though the atoms are not arranged periodically, as in crystals, the hierarchic arrangement causes scattering that is as coherent as in crystals, and as sharp. However, after quasi-structure-factor calculation (**Appendix 1**), the indexed ordering of the diffraction pattern is not integral as in Bragg scattering; but irrational (**Appendix 1**, Figure A2). Moreover, the Bragg-like *rational parts* are separable, in mathematics, from the *irrational parts*. The latter part may be represented by the imaginary part of Euler's wave (**Appendix 2**, Equation (A.2.1), second exponent). The consequent phase shift in the probe forms a universal metric that is, owing to a special mathematical property (Equation (A.1.6)), the same for all of the beams diffracted from a quasicrystal [1] [2]. The quasi-Bloch wave that is used in QC diffraction analysis is a stretched form (red wave in Figure 2) of the periodic Bloch wave (blue) that describes alternative image formation in *crystals*. Notice that the quasi-Bloch wave is commensurate with the logarithmic intercepts (central line in Figure 2) and also, because of dual linearity, is periodically commensurate about each intercept. Moreover, the log-lin metric reveals a special property of the Fibonacci sequence F(1, τ).

The dual log-lin solution for the two types of pattern in CBED in QCs is given here for the first time. It complements and confirms the earlier general solution for the logarithmic patterns in earlier parallel beam diffraction. Previously, this solution seemed complete in the sense that it described uniquely both the structure of the QC, together with its unique diffraction mechanism. We now confirm that apparent "completeness", by the additional explanation for simultaneous logarithmic and linear patterns appearing in the *convergent* beam diffraction.

This analysis has general consequences for quantum physics: the quantization occurs simultaneously in both logarithmic and linear spaces. The mechanism unites dual resonances that are enabled by dual harmonies in the hierarchic scattering structure. The mechanism is enabled by the log-lin metric that is, apparently, unique to the icosahedral symmetries. Moreover, the diffraction is both quasi-Bragg and dynamical diffractive. This complicated set of patterns is not explained by chance: when the quantum is *axiomatic*, it is formless *math*; but as *physical*, the data demonstrate multi-faceted *resonance*.

3. Conclusions

The log-lin metric, that was previously discovered to explain the novel logarithmic periodicity in *quasi-Bragg diffraction* patterns of a hierarchic structure, is now extended and confirmed by consistent explanation of even more complicated *convergent beam electron diffraction* in the quasicrystals. The consistent quasi-Bloch waves, that were logarithmically periodic within the hierarchic structure in parallel beam diffraction, are now simultaneously diffracted in CBED by dynamical diffraction in linear order.

More generally, this description, in simultaneous linear and logarithmic diffraction spaces, *i.e.* momentum spaces, reflects on the nature of the quantum in physics. Whatever mathematicians may axiomatize or define, in quasicrystal physics, the momentum quantum is a resonant state, *i.e.* a transition state between *harmonic states*. In CBED, the transition is resonant in two spaces with multiple, complicated, dual properties: this is what the *physical quantum* does. The same explanation applies to quanta in energy space, and in other spaces: magnetic, thermal, wave band, etc. The explanation applies even to wave function collapse [14] as physical[5]; not just axiomatic.

Conflicts of Interest

The author declares no conflicts of interest regarding the publication of this paper.

References

[1] Bourdillon, A.J. (2020) Complete Solution for Quasicrystals. *Journal of Modern Physics*, **11**, 581-592. https://doi.org/10.4236/jmp.2020.114038

[2] Bourdillon, A.J. (2011) Logarithmically Periodic Solids. Nova Science.

[5]According to Penrose, R. (2024), "Roger Penrose Thinks Quantum Mechanics is Dead Wrong", (https://www.Youtube.com/watch?v=HPH-SzWF46w).

[3] Bourdillon, A.J. (1987) Fine Line Structure in Convergent-Beam Electron Diffraction of Icosahedral Al_6Mn. *Philosophical Magazine Letters*, **55**, 21-26. https://doi.org/10.1080/09500838708210435

[4] Bourdillon, A.J. (2023) Quantum Mechanics: Harmonic Wave-Packets, Localized by Resonant Response in Dispersion Dynamics. *Journal of Modern Physics*, **14**, 171-182. https://doi.org/10.4236/jmp.2023.142012

[5] Von Neumann, J. (1932) Mathematical Foundations of Quantum Mechanics [Mathematische Grundlagen der quantenmechanik]. Spinger.

[6] Popper, K.R. (1982) Quantum Theory and the Schism in Physics. Hutchinson.

[7] Popper, K.R. (1980) The Logic of Scientific Discovery. Hutchinson.

[8] Bourdillon, A.J. (2013) Icosahedral Stereographic Projections in Three Dimensions for Use in Dark Field TEM. *Micron*, **51**, 21-25. https://doi.org/10.1016/j.micron.2013.06.004

[9] Shechtman, D., Blech, I., Gratias, D. and Cahn, J.W. (1984) Metallic Phase with Long-Range Orientational Order and No Translational Symmetry. *Physical Review Letters*, **53**, 1951-1953. https://doi.org/10.1103/physrevlett.53.1951

[10] Steeds, J. and Mansfield, J. (1984) Convergent Beam Electron Diffraction of Alloy Phases. Hilger.

[11] Tanaka, M. and Terauchi, M. (1985) Convergent Beam Electron Diffraction. JEOL Ltd.

[12] Hirsch, P., Howie, A., Nicholson, R.B., Pashley, D.W. and Whelan, M.J. (1977) Electron Microscopy of Thin Crystals. Krieger.

[13] https://www.xraylithography.com

[14] Bourdillon, A.J. (2024) Quantum Mechanics: Collapse. UHRL.

[15] Bleaney, B.I. and Bleaney, B. (1965) Electricity and Magnetism. Clarendon.

[16] Bourdillon, A.J. (2024) Where Is Phase Velocity in Minkowski Space? *Journal of Modern Physics*, **15**, 1555-1566. https://doi.org/10.4236/jmp.2024.1510065

[17] Bourdillon, A.J. (2023) Quantum Mechanics: Internal Motion in Theory and Experiment. *Journal of Modern Physics*, **14**, 865-875. https://doi.org/10.4236/jmp.2023.146050

[18] Bourdillon, A.J., Boothroyd, C.B., Kong, J.R. and Vladimirsky, Y. (2000) A Critical Condition in Fresnel Diffraction Used for Ultra-High Resolution Lithographic Printing. *Journal of Physics D: Applied Physics*, **33**, 2133-2141. https://doi.org/10.1088/0022-3727/33/17/307

[19] Jenkins, F.A. and White, H.E. (1976) Fundamentals of Optics. McGraw-Hill.

[20] Bourdillon, A.J. and Vladimirsky, Y. (2002) Ultra High Resolution Lithographic Imaging and Printing by Exposure Near the Critical Condition. US Patent 6383697.

[21] Bourdillon, A.J. and Vladimirsky, Y. (2006) X-Ray Lithography—On the Sweet Spot. UHRL.

Appendix

Appendix 1. Logarithmic Diffraction in Quasicrystals

Figure A1 illustrates chief differences between high energy electron diffraction in crystals versus quasicrystals. The upper row models a crystal with periodic, face-centered cubic unit cells. Like the X-ray probe, an electron probe is periodic. When it is directed parallel to the [100] axis of the crystal which is also periodic, the resulting diffraction is likewise periodic. The pattern is observed as an image of the back focal plane of the microscope objective lens.

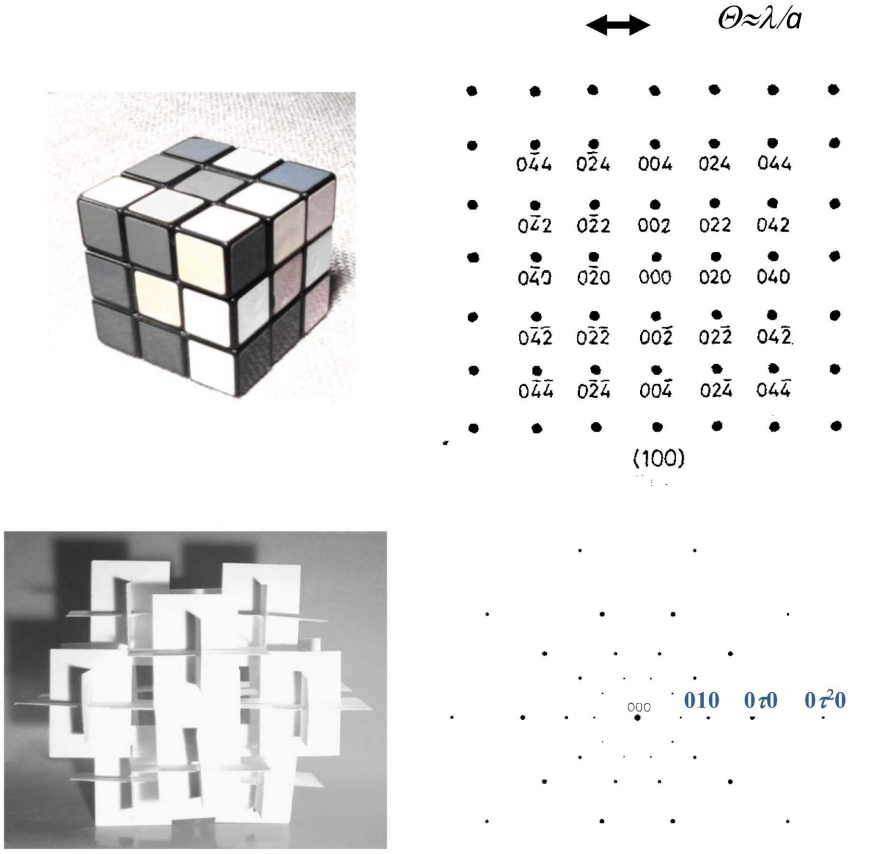

Figure A1. *Upper figures*: cubic structure and face-centered cubic diffraction pattern normal to the [100] axis. The probe, the crystal and the pattern are all periodic. *Lower figures*: the hierarchic quasicrystal and corresponding diffraction pattern normal to the fivefold [τ01] axis. The pattern is icosahedral in geometric space. The pattern and structural cells are in geometric series, with stretching factor between orders τ^2. The double arrow represents a momentum quantum.

The quasicrystal is not periodic, nor does it obey Bragg's law of crystal diffraction. *A priori*, relationships between probe wavelength λ, angle of incidence θ, interplanar spacing d, were unknown. By assuming initially a dense unit cell and a hierarchic icosahedral structure, scattering is simulated with the quasi-structure factor S_{hkl} for the diffraction beam indexed (h, k, l). Calculate S_{hkl} first for the cell and later for the (whole) quasicrystal.

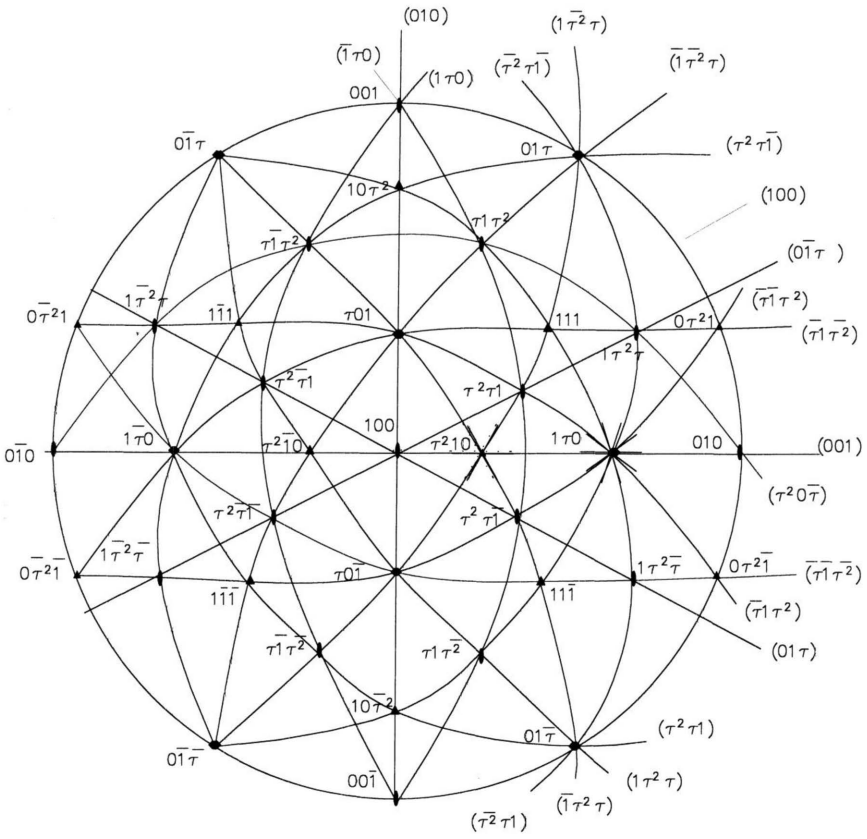

Figure A2. Stereogram of principal axes of the icosahedral structure, and through them, atomic plane normals. Both axes and plane normals are 3-dimensional and ordered in irrational, geometric series.

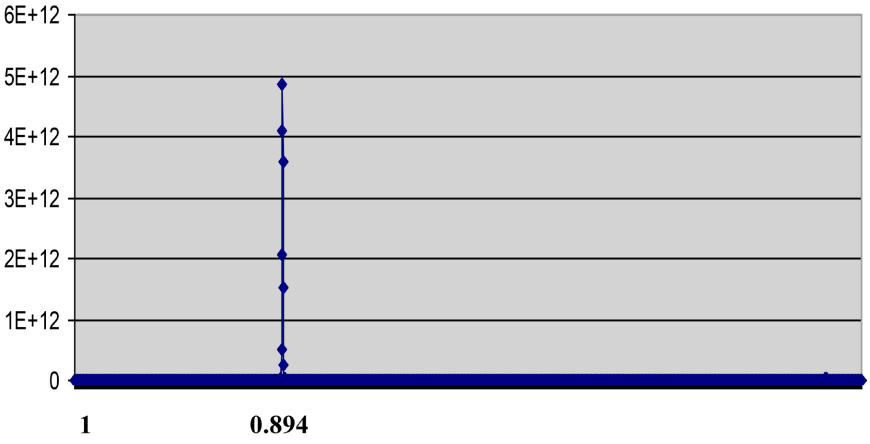

Figure A3. Computed Quasi-Structure Factor (ordinate axis) plotted against varying c_s (abscissae) (Equation (A.1.2)) for diffraction of a [τ01] incident beam onto the (0τ0) plane in an Al_6Mn quasicrystal, hierarchic order 6 ([13], p. 30). The offset of the Quasi-Bragg peak (at fractional divergence, $c_s = 0.894$) from the corresponding Bragg condition ($c_s = 1$) of the same Bragg interplanar-spacing is $c_s = 0.894 = (t - 1/2)^{-1}$. This offset is due to the contribution to the scattering offset made by the irrational part of the scattering index. The fact that the diffraction is not Bragg like is a serious departure from conventional physics.

$$S_{hkl} = \Sigma_i^{\text{unit cell}} f_i \cos\left(2\pi c_s \left(\boldsymbol{h}_{hkl} \cdot \boldsymbol{r}_i\right)\right) \tag{A.1.1}$$

where f_i is the atomic scattering factor for atom i, with $\boldsymbol{r}_i$ its location projected onto Bragg plane normal $\boldsymbol{h}_{hkl}$. Meanwhile c_s is a coherence factor that accounts for the multiplanar atomic spacing d and non-planar wave front [1]. For the whole quasicrystal, restricted to 6 hierarchic orders for practical reasons:

$$S_{hkl}^{p} = \Sigma_{hkl}^{p-1} \Sigma_{cc}^{12} \cos\left(2\pi c_s \left(\tau^{2p} \boldsymbol{h}_{hkl} \cdot \boldsymbol{r}_{cc}\right)\right) \tag{A.1.2}$$

where τ^{2p} is the hierarchic stretching factor. Because the unit cells are hierarchically structured, and not periodically repeating, they are added over the whole quasicrystal by summing over cell centers cc order p (the unit cell is counted as the first order). There are 12 sub-clusters in each cluster. For the whole quasicrystal, $S_{0\tau 0}$ is illustrated numerically in **Figure A3**, wherein c_s is scanned away from its unit value in the Bragg condition.

The coherence factor is c_s found theoretically by separating the irrational part of the index which is applied as a phase shift in Euler's wave formula (Equation (A.2.1) in **Appendix 2**). The most extraordinary fact is that c_s is the same for all orders of all diffracted beams recorded from the quasicrystal. It is a new constant in physical atomic structures. It is easily proved by mathematical induction that:

$$\tau^m = F_m\left(1,\tau\right) = \partial_{(m,1)} + F_{m+1}\left(0,1\right) + F_m\left(0,1\right)\tau \tag{A.1.3}$$

where $F_m\left(1,\tau\right)$ is the Fibonacci sequence, seeded $\left(1,\tau\right)$. For example:

$$\tau^5 = F_5\left(0,1\right) + F_6\left(0,1\right)\tau = F_6\left(1,\tau\right) \tag{A.1.4}$$

The formula is separable into natural and irrational parts by substitution of τ for the nearby natural number 3/2, so that:

$$\tau^m = F_m\left(0,1\right) + F_{m+1}\left(0,1\right)\frac{3}{2} + \text{irrational part} \tag{A.1.5}$$

Then the log-lin metric function is constructed from the irrational part that represents the phase shift in Euler's formula (second exponent in A.2.1.) consistent with the numerical displacement from the Bragg Condition for crystals c_s, in **Figure A3**:

$$c_m = \frac{1}{c_s} = 1 + \frac{\tau^m - F_{m+4}/2}{F_{m+1}} = \frac{1}{0.894} = \tau - \frac{1}{2} \tag{A.1.6}$$

i.e. the same, both numerically and theoretically, for all indices and all diffraction orders[6]. Indeed, the phase shift causes the divergence from the Bragg angle in **Figure A3**, and knowledge of the shift enables measurement of the quasi-lattice parameter:

$$d = \frac{\lambda}{2\sin\left(\theta\right)}\tau \cdot c_s \tag{A.1.7}$$

[6] *The Log-lin Metric for Generic Responses in Logarithmic Structures,* Bourdillon A.J., UHRL, APS March Meeting (2015), abstract id. W15.014B, Bibcode: 2015APS.MARW15014B, © The SAO Astrophysics Data System, Mail: adshelp[at]cfga.harvartd.edu. The ADS in is operated by the Smithsonian Astrophysical Observatory with Harvard/Princeton under NASA Cooperative Agreement 80NSSC21M0056.

including the Bragg equivalent $\lambda/(2\sin(\theta))$ [3][7], the line index, and metric function. This is equal to the short side of the golden rectangles in **Figure A1**, lower row. The measurement in turn verifies the quasicrystal structure which locates an Al atom at each rectangle corner, diameter ~0.295 nm. was measured on the (τ00) line [3] and now corrected for the metric function and index [1]. The chief uncertainty in the measurement was due to variations in Mn impurities in second phase Al, that was used to measure camera length. Though it was measured on one specimen by electron energy-loss spectroscopy, the distribution on various second phase crystals could not, at the time, be measured. Estimated uncertainty is ±0.002 nm.

The unit cell contains 15 identical cross-sections, so the quasicrystal resembles a packing of extremely dense quasi-spheres. The packing is presumably defective, with vacancies in lower orders and interstitials at higher orders.

It is of course essential in physics to model the structure and measure it. For the quasicrystal, we had also to model the diffraction process and measure it in its uniqueness. Any other way is make-believe.

Appendix 2. Phase, Energy, and Momentum in Free Wave-Particles

In quantum mechanics, particles have properties of angular frequency ω and wave vector k that are proportional to macroscopic energy and momentum, respectively. Their ratio (equal to the product of frequency f and wavelength λ) is the phase velocity of a photonic or particulate wave. Their values in particular circumstances can be calculated and measured. The joint values in massive particles multiply to numbers faster than the speed of light which was supposed to be limiting in special relativity. *If phase velocity were a thing*, then it would not be true that "nothing travels faster that the speed of light", in words of common parlance. The explanation for the contradiction starts with the concept of the wave group that is founded on wave-particle duality, including not only the massless quantized photons derived from Maxwell's electromagnetism, but especially all massive particles, including electrons, neutrons, etc.

The simplest group is also a common group in physics, including statistical physics. It is based on the normal distribution in the wave function (**Figure A4**):

$$\varphi = A\cdot\exp\left(\frac{X^2}{2\sigma^2}+iX'\right)$$

$$\text{with imaginary:}\quad X = i\left(\bar{\omega}t-\bar{k}x\right);\quad X' = i\left(\omega t-kx\right) \tag{A.2.1}$$

where A is a normalizing constant; σ is proportional to Uncertainty (**Appendix 3**)[8]; and t and x represent respectively time and position, shown here in one spatial dimension, for simplicity. The imaginary factor X contains mean values of angular

[7]Tsai, A.P. made the same measurement, but without the corrections for index and metric, in *Sci. Technol. Adv. Mat.* **9** 1-20, (2008).

[8]$\Delta t = 2\sigma/\bar{\omega}$; $\Delta\omega = 4\bar{\omega}/\sigma$; $\Delta x = 2\sigma/\bar{k}_x$; $\Delta k_x = 4\bar{k}_x/\sigma$; $\Delta\omega\cdot\Delta t = 8$, $\Delta x\cdot\Delta k_x = 8$ etc. *i.e.* 16 times greater than Heisenberg's "limits".

frequency $\bar{\omega} = 2\pi f$ and of wave vector $\bar{\boldsymbol{k}} = 2\pi/\lambda$. They stabilize the normal envelope function in free space and X' represents the variables in Euler's plane wave. This wave is two dimensional for simplicity, but is extensible to include also the two dimensions of the transverse plane.

The energy of this wave is given by $E = \int\left(\boldsymbol{E}^2/2\varepsilon_o + \boldsymbol{H}^2/2\mu_o\right)\mathrm{d}\tau$ in Maxwell's theory. For emission from a vertical dipole, the electric field $\boldsymbol{E}$ is then vertical as in Figure A4 and the magnetic field $\boldsymbol{H}$ horizontal. The constants ε_o and μ_o represent respectively, the electric permittivity and magnetic permeability of free space. With quantization due to a resonating emitter, $E_n = \hbar\omega_n$ as in Planck's law, owing to harmonic emission to be described further in **Appendix 3** below. We define the uncertainty of the wave as its full width, $1/e$ of max.

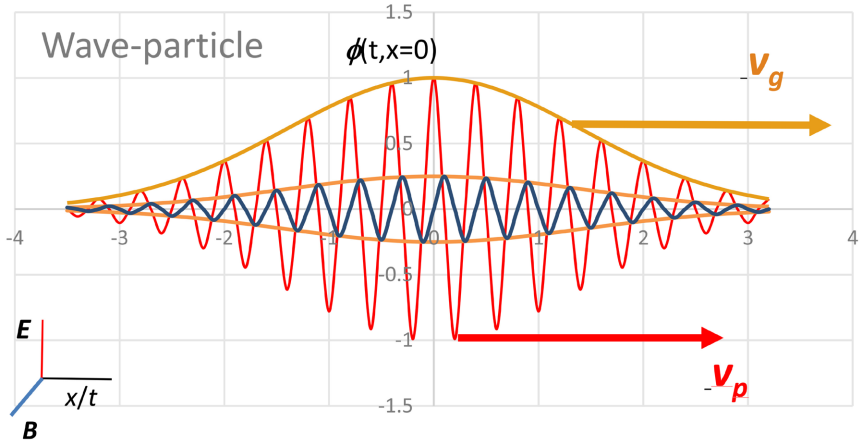

Figure A4. Normal wave packet including conservative function (orange) enveloping infinite, responsive, complex wave (red and blue), with uncertainty s (pink double arrow) at time $x = 0$. The Fourier transform of a Gaussian is Gaussian, so *the abscissae* may represent any of the four variables x, k_x, t, or ω. In massive particles, the group velocity $v_g < c$ (orange, distance travelled per unit time); the phase velocity $v_p > c$ (red). Applying the packet to electromagnetism, if the real part Re(ϕ) represents real $\boldsymbol{E}$, the imaginary part Im(ϕ) represents real $\boldsymbol{H}$.

Equation (A.2.1) is a solution for Maxwell's wave equations in electromagnetism, where, in free space $\nabla^2\boldsymbol{E} = \varepsilon_o\mu_o\left(\partial^2\boldsymbol{E}/\partial t^2\right)$, while $\nabla^2\boldsymbol{H} = \varepsilon_o\mu_o\left(\partial^2\boldsymbol{H}/\partial t^2\right)$ ([15] p. 263). Because the wavefunctions for light in optical microscopes are reproduced, in all principal ways, in electron microscopes (excepting minor differences of polarization in light versus mass, charge and spin on the electron), we can apply formula (A.2.1) as the alike wavefunction for the free electron.

By comparing classical dynamics with relativistic dynamics, where mass varies with energy dependence, we can introduce and derive expressions for phase velocity and group velocity.

In 1905, Einstein discovered that physical laws are invariant in all inertial reference frames. This includes the universal speed of light in free space, $c = \left(e_o \cdot \mu_o\right)^{-1/2}$. From this fact he determined the equivalence between energy E

and relativistic mass, $E = m'c^2 = \gamma m_o c^2$ (*i.e.* including kinetic energy and the Lorentz factor $\gamma = \left(1 - v_g^2/c^2\right)^{-1/2}$, and furthermore $E^2 = \boldsymbol{p}^2c^2 + m_o^2c^4$, where $\boldsymbol{p}$ is the 3-dimensional momentum of a particle that has rest mass m_o. After applying Planck's law, $E = \hbar\omega$, and the de Broglie hypothesis in terms of wavevector, $p = \hbar k$, the equation yields [1]:

$$\omega^2 = k^2c^2 + m_o^2c^4/\hbar^2 \tag{A.2.2}$$

in one dimension for simplicity. By writing in natural units $\hbar = 1 = c$, m_o is a wave-particle since $m_o = \pm\sqrt{\omega^2 - k^2} = \pm\sqrt{(\omega - k)(\omega + k)}$. The function in $(\omega - k)$ oscillates in time or space; while $(\omega + k)$ conserves the physical properties of the particle. Differentiation of Equation (2) yields the very important result:

$$\frac{\omega}{k}\cdot\frac{\mathrm{d}\omega}{\mathrm{d}k} = c^2 \quad \text{and} \quad \frac{\mathrm{d}\omega}{\mathrm{d}k} = \frac{c^2}{v_p} \tag{A.2.3}$$

Waves are common in fluid phases of matter because they move more easily than solid bodies of equivalent mass. The velocity of a wave is given by its wavelength λ that oscillates at frequency f per second [16] [17]:

$$v_p = \lambda\cdot f = \frac{\omega}{k} \tag{A.2.4}$$

The *group velocity* $v_g = \mathrm{d}\omega/\mathrm{d}k$ will be derived below. The product $v_p \cdot v_g = c^2$ is constant.

In the bunched quantum, the second velocity generated is slower than this phase velocity: the *group velocity* v_g is related to the beat frequency that is familiar to piano tuners when sound waves superpose. It is also related to the resonant frequency of a bridge, known to marching soldiers who are ordered to, "break step" when approaching it: the break avoids the resonant strain and failure of the bridge. It turns out that resonance is a common feature in physics generally, but this is especially the case in quantum physics. We will show that, typically, the resonance occurs at emission; or at scattering; or at measurement; and is transmitted in the bunched quantum—the same quantum that was proved, by Planck and Einstein, to be a property of electromagnetic radiation. By comparing classical dynamics with relativity, we show how, algebraically, to represent the group velocity:

At low (*classical*) energies, *i.e.* $E \approx E_0$; so that:

relativistic mass, $m' \approx m_o$; and $\hbar k \ll m_o c$ while rest energy:

$$E_o = m_o c^2 \text{; and dynamically}^9, \quad E \approx m_o c^2 + \frac{p^2}{2m_o} \tag{A.2.5}$$

while momentum:

$$p = m_o v \approx \frac{E_o}{c^2}\cdot v_g \quad \text{or by re-arranging} \quad v_g \approx \frac{pc^2}{E_o} \tag{A.2.6}$$

[9]First order Binomial approximation of the relativistic $E = \sqrt{p^2c^2 + m_o^2c^4}$ implies $E \approx m_o c^2 + p^2/2m_o$ when $p \ll m_o c$.

Then, by application to any energy, since *E and m′ increase* with increasing momentum, *while* v_g *tends to the constant c*, *E replaces* E_0 *in the classical equation* (A.2.6):

$$v_g = \frac{pc^2}{E} = \frac{\hbar kc^2}{\hbar\omega} = \frac{c^2}{v_p} = \frac{\mathrm{d}\omega}{\mathrm{d}k} \tag{A.2.7}$$

Equation (A.2.7) *defines generally the derivative* $\mathrm{d}\omega/\mathrm{d}k = v_g$. Following (A.2.3) in massive particles, reduced group velocity is the inverse of reduced phase velocity:

$$\frac{v_g}{c} = \frac{c}{v_p} \tag{A.2.8}$$

and this is equally true in massless particles where: $v_p = c = v_g$. Emphatically, de Broglie's quantized momentum is proportional to the *group* velocity, $v_g \propto \mathrm{d}\omega/\mathrm{d}k$; in contrast to Planck's quantized energy that is proportional to *phase* velocity, $v_p \propto \omega/k$. These properties are consequences of relativity. Notice that because *c* is invariant in all inertial reference systems, then if v_g is identical by complementarity in any two reference frames, v_p is also identical. Moreover, the phase velocities in the transverse plane, v_p^y and v_p^z, can be surprisingly large. In that case, they should affect scattering factors and cross-cross-sections even when v_p^x is strongly relativistic.

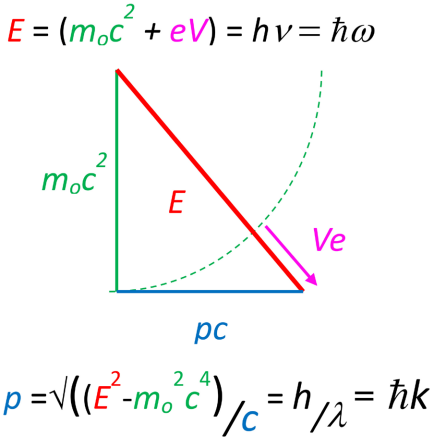

Figure A5. The frequency *n* and wavelength λ of an electron microscope probe are related by Pythagoras' theorem as in relativity (Equation (A.2.2)). The probe energy is the electron rest mass energy plus the accelerating energy of the gun, *Ve*.

Figure A5 and **Figure A6** show, for free electrons, logarithmic plots of *f*, λ, v_g and v_p, *etc*. when the acceleration energy of an electron varies from 10 volts to 10^8 volts. These plots were calculated by starting with the Pythagorean relationships in formula (A.2.3) [14]. However, most of the numbers calculated—including the group velocity that is used in special relativity—are the same as can be found in electron microscope handbooks (e.g. [13]). They are therefore virtually experimental because of constant and consistent usage over a period approaching 100

years:

$$E = \left(m_o c^2 + eV\right) = hf = h\omega \tag{A.2.9}$$

as in Planck's law, and under de Broglie's hypothesis:

$$p = \frac{\sqrt{E^2 - m_o^2 c^4}}{c} = \frac{h}{\lambda} = \hbar k \tag{A.2.10}$$

Equations (A.2.9) and (A.2.10) provide the values for f and λ that are illustrated in Figure A6.

The wave group describes the probe that we use in the electron microscope.

The phase velocity v_p is assertive in bound states where harmonic resonance overlaps peaks from successive cycles in time, at high repetition rates.

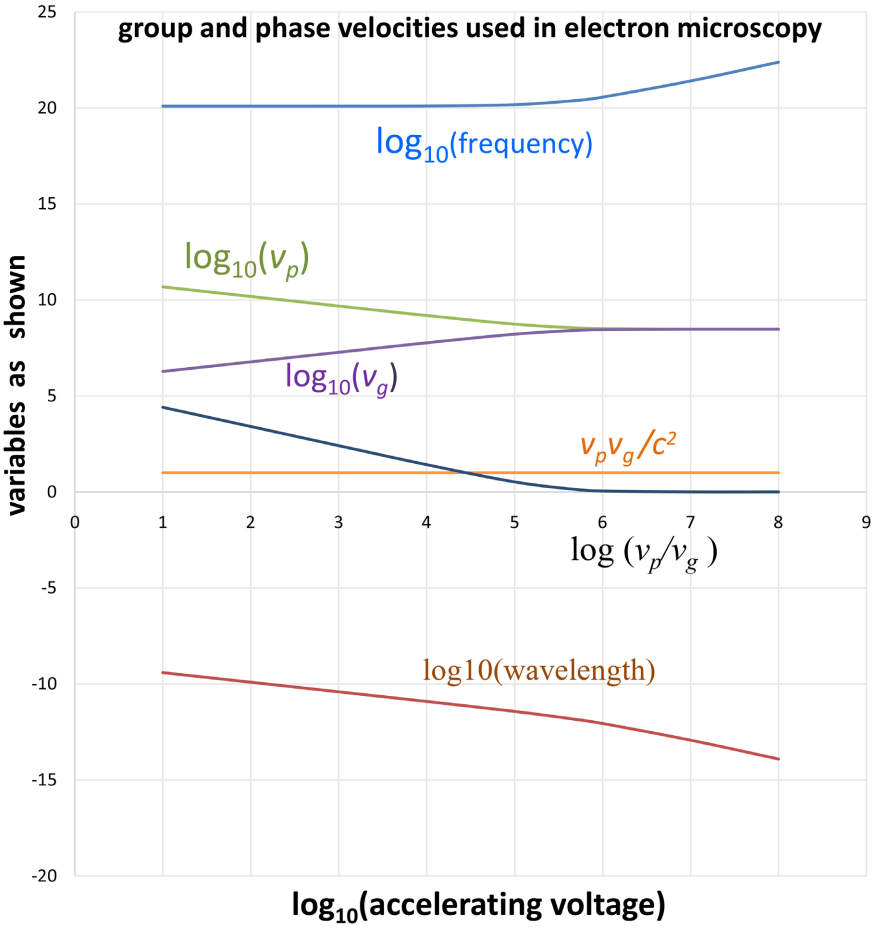

Figure A6. Values for parameters in various electron probes plotted against acceleration energies between 10^1 to 10^8 eV, including from top down: the frequency (blue) in SI units; the phase velocity v_p (green), the group velocity v_g (purple); the ratio of phase/group velocities (navy blue); the product of phase with group velocities (yellow); and the wavelength (red). Notice the systematic relativistic changes when $Ve \simeq m_o c^2 \simeq 0.5$ MeV, excepting only the constant product $v_p v_g$[10].

[10]The dispersion dynamics for free-wave-particles [20] applies also to: magnetism. spin, magnetic radius, Meissner effect, superconductivity, tunneling, mass, entanglement, conservation laws, symmetry, transverse phase etc. [13] [16].

Appendix 3. Certainty

Heisenberg's uncertainty that is used in mathematical quantum mechanics is consistent with minimum action and is sometimes used to interpret interference properties in wave-particle duality, *i.e.* where superpositions of waves add in some places to zero. This representation allows for a "point particle" by assumption. Moreover in measurement, collapse of the wave function is considered "instantaneous and indeterminate" in mathematics, as though integration is not made over time, and contrary to methods in physical experimentation.

By contrast, when we adopt the wave group (Equation (A.2.1)) as the realistic and physical representation, the "uncertainty" extends in those regions beyond full width half maximum (or 1/e) of the wave function. Our limit is 16 times greater than Heisenberg's limit (**Appendix 2**). Moreover, measurement is itself a physical process, and includes for example contemporaneous emission and annihilation [14] in the wavefunction collapse in Young's slit experiments.

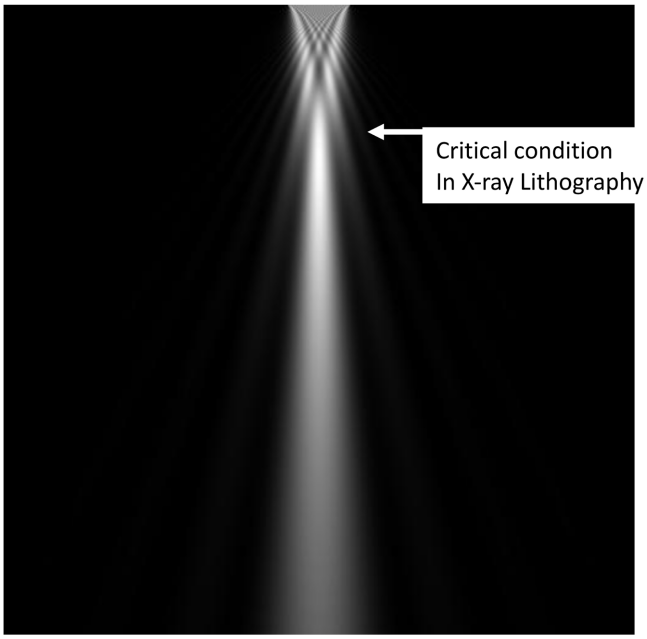

Figure A7. Simulation of 100 keV electron beam transmitted by a narrow slit. Notice the variations from near field to far field imaging in Fresnel diffraction: Δx is minimum at the critical condition, with Δp_x passing from negative (converging) to positive (diverging). At the experimental critical condition, the dual uncertainty is 4 x larger than at Heisenberg's "limit". The critical condition corresponds to the extremum width in Cornu's spiral [18]-[20]. Simulation due to C.B. Boothroyd.

Fresnel knew, about wave behavior 100 years before Heisenberg. For example, **Figure A7** illustrates the wavefunction for electron waves transmitted through a narrow slit [18]. The wavefunction closely resembles the wavefunction described by Fresnel for light waves [19]. In both cases, for light and for the electrons, the near field condenses the transmitted beam and then expands it in the far field. These features are experimentally confirmed. They contradict the comparatively

vague assertions of Heisenberg's uncertainty. In particular, the cross-over from near to far fields corresponds to the extremum in Cornu's spiral (**Figure A8**) that is used to define the "critical condition" [18] [20] [21] in X-ray lithography. This condition is experimentally confirmed, and unknown in the Heisenberg interpretation. Uncertainty is a critical feature of the probe wave function that we use to understand the CBED diffraction[11].

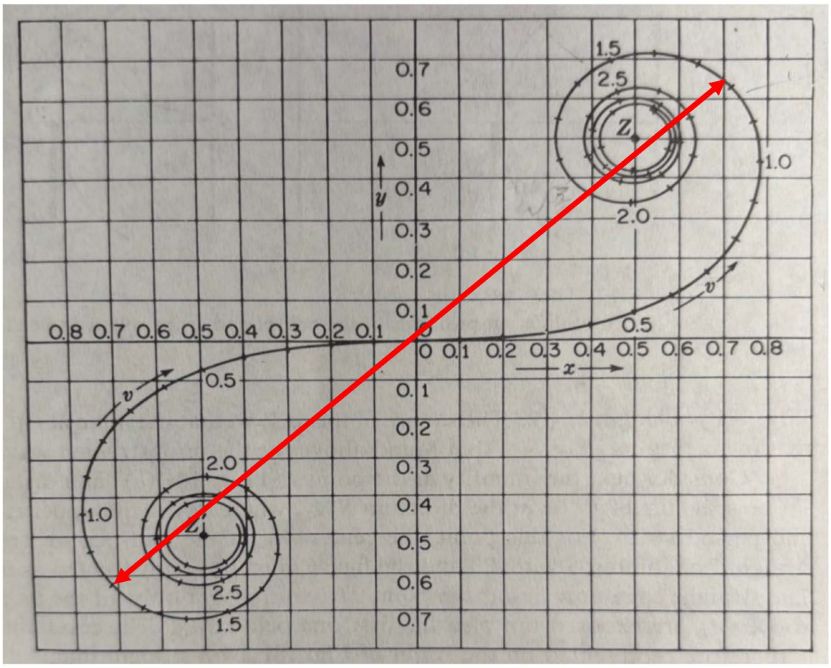

Figure A8. The critical condition in X-ray lithography occurs when the proximity image is minimum at the intersection of near field and far field, *i.e.* at the extremum in Cornu's spiral (red arrow). This dual uncertainty is 4 times greater than Heisenberg's limit.

[11]Heisenberg's Uncertainty can hardly be wrong since *his* "limit" is small enough; what physicists need is the expected uncertainty, most notably when circumstances are defined, e.g. for free particles or thin slits or impact parameter calculations [12] [Bourdillon, A.J., (1984) *Phil. Mag.* **A-50** 839-848].